Self-optimisation of Continuous Flow Electrochemical Synthesis Using FTIR and Gas Chromatography

Jie Ke[a], Chuang Gao[a,b], Ana A. Folgueiras-Amador[c], Katherine E Jolley[a,c], Oscar de Frutos[d], Carlos Mateos[d], Juan A. Rincón[d], Richard C.D. Brown[c], Martyn Poliakoff[a] and Michael W. George*[a,b]

[a]School of Chemistry, University of Nottingham, University Park, NG7 2RD, UK

[b]Department of Chemical and Environmental Engineering, The University of Nottingham Ningbo China, 199 Taikang East Road, Ningbo 315100, China

[c]School of Chemistry, University of Southampton, Highfield, Southampton SO17 1BJ, UK

[d]Centro de Investigación Lilly S.A., Avda. de la Industria 30, 28108 Alcobendas-Madrid, Spain

E-mail: mike.george@nottingham.ac.uk

Abstract

A continuous-flow electrochemical synthesis platform has been developed to enable self-optimisation of reaction conditions of organic electrochemical reactions using Attenuated Total Reflection Fourier-Transform Infrared Spectroscopy (ATR-FTIR) and Gas Chromatography (GC) as online real-time monitoring techniques. We have overcome the challenges in using ATR-FTIR as the downstream analytical methods imposed when a large amount of hydrogen gas is produced from the counter electrode by designing two types of gas-liquid separators for analysis of the product mixture flowing from the electrochemical reactor. In particular, we report an integrated gas-liquid separator with an ATR-FTIR probe at the reactor outlet to give a facile and low-cost solution to determining the concentrations of products in gas-liquid two-phase flow. This approach provides a reliable method for quantifying low-volatile analytes, which can be problematic to be monitored by GC. Two electrochemical reactions, the methoxylation of 1-formylpyrrolidine and the oxidation of 3-bromobenzyl alcohol were investigated to demonstrate that the optimal conditions can be located within the pre-defined multi-dimensional reaction parameter spaces without intervention of the operator by using the SNOBFIT (Stable Noisy Optimisation by Branch and FIT) algorithm.

Introduction

There is an ever-increasing use of computers and digitisation in manufacturing as exemplified by *Industry 4.0*, a strategic initiative recently introduced by the German government, which aims to transform industrial manufacturing via digitisation and exploitation of new technologies.[1] The use of automation in the chemical industry has, in part, been facilitated by the recent drive in the pharmaceutical industry to switch from traditional batch reactors to continuous processing for the manufacture of active pharmaceutical ingredients (APIs)[2, 3] together with the ever-increasing application of Process Analytical Technology (PAT)[4] particularly for initiatives such as Quality-by-Design (QbD).[5]

Traditionally, pharmaceuticals have been made by a sequence of batch reactions with isolation of solid intermediates before the isolation of the desired end-product. However, continuous manufacturing has great potential for improving agility, flexibility, and robustness in the manufacture of pharmaceuticals. Furthermore, continuous flow processes are particularly suited to automation with technical advances and greater availability of in-line analytical approaches. PAT is already widely used for monitoring reactions in continuous flow systems with increased activity in automated self-optimisation where a computer-controlled continuous reactor, in-line/on-line analysis and optimisation algorithms are combined to adjust reaction conditions automatically to optimise the outcome of the reaction. A variety of real-time inline spectroscopic and analytical PAT tools have been used for self-optimisation including both chromatographic (GC and HPLC/UPLC) and spectroscopic (UV/Vis, Raman, IR, and NMR) approaches.[6] Early work in this area combining reactor control with feedback algorithms included the optimisation of nanoparticle production with online fluorescence,[7] and online HPLC analysis for optimisation of Heck coupling[8] and Knoevenagel condensation.[9] Some of us demonstrated the versatility of self-optimisation of the reaction of dimethyl carbonate and 1-pentanol in supercritical CO_2 ($scCO_2$) to form pentyl methyl ether where optimisation could be used to maximise/minimise any one of a range of different criteria (i.e., yield, space-time yield, E factor or a weighted yield function).[10] Self-optimisation continues to develop rapidly and the area has been regularly reviewed.[11-17] Indeed, a special issue on *Synthesis 4.0: Towards an Internet of Chemistry*[18] highlighted recent developments in the area of self-optimisation and machine learning including automated platforms for flow processes,[19] integration of multiple PAT tools for multistep reaction,[6] obtaining kinetic information,[19-21] algorithms for the self-optimisation,[22] and uniting laboratory automation, DoE data, and modelling techniques together to accelerate chemical process development.[23] More specifically, there has been a recent explosion in activity in flow chemistry and continuous manufacturing, including both photochemistry[24-31] and electrochemistry.[32-35] This is partly because these can be considered *"reagentless"* methodologies, offering

milder approaches to obtaining highly reactive intermediates, providing access to structurally complex molecules and scaffolds that can be difficult to obtain using more "traditional" approaches.

Electrochemistry allows redox chemistry to occur using electrons as traceless reagents as well as potentially avoiding the use of hazardous and toxic reductants and oxidants. There is also scope to use potentials and currents to tune reactivity and maximise selectivity. In addition, flow electrochemistry offers the possibility of utilising sustainable electricity, derived from solar and wind energy. Up to now, however, there have been relatively few reports of self-optimisation being applied to flow photochemical and electrochemical processes, not least because electrosynthesis often generates large volumes of gas as a counter-electrode reaction, which can hinder in-line sampling.[36-38]

Over the past a few years, we have developed a number of self-optimising reactors[10, 39-44] to study the chemical reactions at elevated temperature and pressure, including dehydration of ethanol,[43] methylation of alcohols with dimethyl carbonate,[39] and N-alkylation of amino alcohols.[44] We have used on-line monitoring with a computer-controlled sampling valve to reliably transfer samples from supercritical CO_2 streams to the GC injector. In this paper we build upon these studies to probe electrochemical reactions using GC and ATR-FTIR for a reaction that generates H_2 gas and describe how to obtain consistent chromatographic and spectroscopic data from solutions containing copious amounts of gas bubbles.

EXPERIMENTAL

As reported in our previous work [39-44] and the other studies, [45-47] a self-optimising continuous-flow reactor usually consists of three main parts: (i) fluid delivery unit, (ii) the reactor(s) and (iii) an analytical instrument(s) to provide input(s) for the optimisation algorithm. A key factor is the choice of an appropriate analytical method, which primarily depends on the target analytes, concentration and phase state (gas or liquid) of the reaction mixture emerging from the reactor. When the analytes of interest are sufficiently volatile, gas chromatography (GC) can be a preferred choice, whereas other analytical methods (e.g. FTIR or Raman) or liquid chromatography (HPLC) are often selected to quantify low volatile analytes. In this paper, we have incorporated both GC and ATR-FTIR into a newly developed self-optimising continuous-flow electrosynthesis system based around the Ammonite flow reactor, [34, 48-50] but the approach is potentially applicable to other electro-flow reactors. The two analytical methods require different sampling strategies.

The fluid delivery unit and the reactor

Figure 1a shows a schematic diagram of the fluid delivery unit and the reactor used in our continuous-flow electrochemical synthesis system, which allows us to vary the concentrations of the substrates and the flow rate. Two computer-controlled HPLC pumps (Jasco, PU-980) independently deliver two solutions to the Ammonite electrochemical reactor (ER) *via* a static mixer (M), consisting of a stainless steel tube of 15 cm in length and ¼ inch in outer diameter, filled with glass beads (Sigma-Aldrich, 425-600 μm). Both solutions have identical concentrations of the supporting electrolyte and of an internal standard (if required) in the same solvent or solvent mixture. The first solution reservoir (S1) contains the substrate with a known high concentration (C_{subs}^{high}); while the concentration of the substrate in the second solution reservoir (S2), is much lower C_{subs}^{low} than that in S1. Prior to the experiments, the flow rate of both pumps (PU1 and PU2) were calibrated using 2-propanol (i.e. measuring the mass of 2-propanol collected over a fixed period of time). Then, for a pre-set value of total flow rate, any concentration of the substrate between C_{subs}^{low} and C_{subs}^{high} can be obtained merely by adjusting the relative calibrated flow rates of the two pumps.

The Ammonite 8 electrochemical reactor (Cambridge Reactor Design Ltd.) is an undivided cell for laboratory synthesis on a multi-gram scale. [34, 48-50] The flow channel is formed by a planospiral groove in the cathode which is then separated from the anode by a complementary spiral polymer gasket.[51] This creates a 100 cm spiral flow path of width 0.2 cm with a 0.5 mm inter-electrode gap giving a channel volume and hence total reactor volume of 1 cm^3. The planospiral shape of the flow path makes the reactor very compact and easy to both use and clean. A computer-controlled, digital DC power supplier (Keithley, 2260B-30-36, denoted as DPS in Figure 1a) controls the current/voltage applied to the Ammonite. The fluid delivery unit and the reactor are common to the two configurations of the downstream unit described below.

Configuration for use with GC

For the electrochemical oxidative reactions described in this study, the counter electrode reaction can produce considerable amounts of H_2 gas as a by-product of the corresponding reductive process e.g. reduction of methanol (MeOH) solvent at the cathode. Thus, assuming 100% current efficiency when feeding a solution of 0.5 mol dm^{-3} of 1-formylpyrrolidine in MeOH into the reactor, the volumetric ratio of the H_2 gas : liquid at the exit of the reactor is 11:1. Therefore, it is essential to find a reliable method to separate the liquid phase from the two-phase gas/liquid flow because any tiny gas bubbles presenting in the GC sample loop can significantly lower the

reproducibility of the GC measurements. Here, we report a new design of a gas-liquid separator (GLS), which can work efficiently with a GC sample injection valve.

The GLS is essentially a T-piece made of Swagelok stainless steel components (Figure 2a), with the T rotated by 90°. The GLS is placed 50 cm vertically above the height of the Ammonite reactor. The two-phase flow (labelled G+L in Figure 2a) enters the GLS along the horizontal part of the T. When it reaches the actual T junction, the gas phase (e.g. H_2) is released from the top; whereas the liquid phase is withdrawn from the lower part of the separator and is then transferred to the GC sample loop using a HPLC pump (PU3). An additional peristatic pump (Cole-Parmer, MasterFlex L/S 07551-20, denoted as PP in Figure 2a) that is connected to the very bottom of the GLS is used to replace the liquid inside the GLS with clean solvent between two GC measurements. There are two problems that have to be addressed (i) the liquid must be as cool as possible to avoid solvent vapour being entrained with the gas phase. This is solved by placing a heat exchanger (HE) to cool the liquid close to the input of the GLS. (ii) The level of the liquid needs to be maintained very precisely in the GLS. If it is too high, liquid can be forced out by the gas bubbles; if it is too low, the gas separation may be incomplete. This problem has been overcome by using a glass tube (GT; 6 mm O.D.) so arranged that the liquid inside it is at exactly the same level as in the opaque steel tube of the GLS. The level in the glass tube is monitored with a liquid-level detector (LLD) built in-house, which consists of a vertical array of 10 optical sensors (OPTEK Technology, OPB350). The outputs from the 10 optical sensors are processed by a computer which then controls the pumping rates of the two pumps (PU3 and PP) to ensure that the liquid level remains constant so that only the liquid phase is transferred to the GC sample loop.

Thus, with the help of the liquid level detector, the H_2 gas can be separated continuously from the liquid phase. Because the total volume of the GLS is relatively large (~10 cm^3), it takes a long wait time (>30 min) to reach a steady-state after new experimental conditions have been set, particularly, when the total flow rate of the reaction mixture is low. This problem has been overcome by introducing a cleaning procedure between two experiments. In this cleaning procedure, the peristaltic pump discharges all of the fluid in the GLS, and then stops for several minutes to let the GLS refill with fresh incoming reaction solution. The cleaning procedure is repeated three times to ensure that the reaction solution being transferred to the sample loop is representative of the latest outcome from the reactor. These three cleaning cycles, carried out automatically by a control program written in LabVIEW, reduce the re-equilibration time to only 10 -15 minutes, depending on the flow rate.

After the reaction solution passes through the GLS, the liquid phase is sampled by a GC injection valve (IV in Figure 1b), which is a four-port, two-position valve (VICI, CI4WE.2) with a microelectric actuator (E90-CE). For each test, the GC sample loop transfers 0.2 μL of the reaction solution to the split/splitless GC injector.

The solution/product reservoirs, the pumps, the Ammonite electrochemical reactor, the gas-liquid separator, etc. are placed in a ventilated box due to the presence of VOCs and possible leaks of H_2 gas. The box also incorporates a pressure transducer (P), an air-flow sensor and a circuit breaker (not shown in Figure 1) to switch off all of the equipment in our self-optimising electrochemical apparatus in the event of over-pressure or of a failure of the air extraction system. No cooling devices have been used to keep the electrochemical reactor at a constant temperature. The typical reaction temperature is between 30 and 40 °C and we have not found any noticeable effects of temperature on product yields in this study.

Configuration for use with ATR-FTIR

For those reaction solutions with analytes of low volatility, IR is a valuable alternative to GC to provide quantitative information on how a chemical reaction proceeds. We used a process IR spectrometer (Mettle-Toledo, ReactIR 702L) equipped with a thermoelectric cooled MCT detector, for which no liquid nitrogen is required, making it particularly suitable for self-optimisation experiments conducted overnight.

The ReactIR spectrometer offers a choice of microflow cell or fibre-conduit ATR immersion probe which we have found to be the more convenient and reliable sampling method because of the large amount of H_2 bubbles in our electrochemical synthesis system. Using the immersion probe, we have designed a simple integrated GLS, illustrated schematically in Figure 2b. The photo of the device is shown in Figure 2c.

The main body of the GLS consists of an inverted-Y shaped piece of glass tubing. The reactor outlet tube carrying the biphasic gas + liquid mixture is sealed into the vertical arm of the Y and extends deep inside it, while the immersion probe of the ReactIR protrudes into one of the side arms of the Y so that it almost meets the reactor outflow. This allows the liquid droplets from the reactor to drip continuously onto the ATR diamond crystal and, since liquids have a high surface tension, the sensing surface of the probe is constantly covered by a thin layer of liquid, the thickness of which is much greater than the IR penetration depth of the ATR-FTIR instrument (typically between 0.5-3 μm).

We have tested the GLS using a two-phase flow with a high gas-to-liquid volumetric ratio over several hours. The collected spectra show no evidence for the gas phase coming into direct contact with the sensing surface during the entire measurements. The tilted configuration for the ATR probe is designed to accelerate the flow of

liquid over the sensing surface, and hence to reduce the waiting time required to obtain reproducible spectra after switching to a fluid with a different composition. The typical waiting time is between 3 to 15 minutes, comparable to the time needed for the electrochemical synthesis reactor to reach a steady state.

To incorporate the integrated GLS into the self-optimising electrochemical synthesis system, we have developed a second configuration of the downstream unit, as shown in Figure 1c. The key feature of the IR configuration is that in addition to the reaction solution, a reference solution can also flow through the integrated GLS for recording an IR background spectrum. A switching valve (Rheodyne, MHP7900-500-1) is installed to select between two solutions. The reference solution is delivered by an HPLC pump (Jasco, PU-980), which can be stopped to reduce the consumption of the reference solution while the spectrum of the reaction solution is being recorded. A peristatic pump (Cole-Parmer, MasterFlex L/S 07551-20, denoted as PP in Figure 1c) is connected to the liquid-phase outlet pipe of the GLS to keep the liquid level well below the sensing surface of the probe. Both the HPLC pump (PU3) and the switching valve (SV) are controlled by a personal computer. With the help of a control software designed in-house, the corresponding IR spectra can be collected first by using the iC IR software for ReactIR (Mettle-Toledo, Version 7.1) and then the data can be transferred to the optimisation software, which will be described briefly below.

Self-optimising reactor software framework

We have recently developed a modular software framework for controlling self-optimising reactors, which can be easily customised as the control software for our self-optimising electrochemical synthesis system in both GC and IR configurations. The primary goal of developing the new software framework was to realise the following functions: (i) allowing plug and play for any analytical instrument; (ii) decoupling the optimisation algorithm and the reactor control/monitoring system; (iii) provision of a generic interface to simplify the development of device drivers; (iv) customisable functions for processing the chromatographic and spectroscopic data; (v) flexible choice of which factors and responses are used by optimisation algorithms.

The software framework has five function modules: (i) device drivers, (ii) rig controller, (iii) chromatography/spectrum processing, (iv) optimisation algorithm, and (v) user interface. The first two modules have been developed using LabVIEW and the remaining three modules have been developed with Matlab. Devices with RS232, USB, or Ethernet ports can be controlled by the rig controller via their corresponding device driver. These devices are not limited to physical devices, but also can be ‘virtual’ devices consisting of a collection of

physical devices (e.g. the downstream unit shown in Figure 1c is a single virtual device comprising a HPLC pump, a switching valve and an FTIR spectrometer).

Chemicals

Tetraethylammonium tetrafluoroborate ([Et_4N][BF_4], Acros, ≥99%), 1-formypyrrolidine (Aldrich, 97%), hexanenitrile (Aldrich, 98%), 3-bromobenzyl alcohol (Flurochem, 99%), 3-bromobenzaldehyde (Alfa Aesar, 97%), acetonitrile (Fisher, HPLC gradient grade, ≥99.9%), methanol (Fisher, analytical reagent grade ≥99.9%) and propan-2-ol (laboratory regent grade, ≥99.5%) were used without further purification. 1-Formyl-2-methoxypyrrolidine was synthesised at the University of Southampton (purity determined by GC and NMR) and was used in Nottingham as supplied.

Results and Discussion

The electrochemical methoxylation of 1-formylpyrrolidine

The methoxylation of 1-formylpyrrolidine, Scheme 1, was chosen as the initial benchmark test for our self-optimising electrochemical reactor because this reaction has already been extensively studied in continuous flow electrochemical reactors and used to characterise their performance.[49, 51]

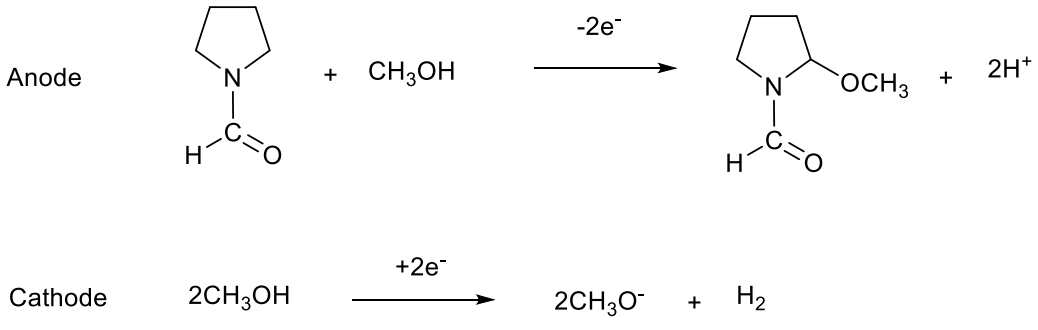

Scheme 1. Electrochemical methoxylation of 1-formylpyrrolidine.

Initially, the reproducibility of the GC analysis was established by pumping 1-formylpyrrolidine (0.1 mol dm^{-3}) and [Et_4N][BF_4] (0.05 mol dm^{-3}) in MeOH at a flow rate of 1 cm^3 min^{-1} over an extended period of time. The working electrode (anode) was a plate of carbon-filled polyvinylidene fluoride with a stainless steel counter electrode (cathode).

Figure 3 shows how a total of 12 tests were carried out at two different currents so as to establish the overall reproducibility. Experiments 1-3 (Group 1) and Experiments 7-9 (Group 3) at a current of 0.16 A, while Experiments 4-6 (Group 2) and Experiments 10-12 (Group 4) at a current of 0.32 A. The peak areas were

integrated for 1-formylpyrrolidine and 1-formyl-2-methoxypyrrolidine, respectively from the GC trace. The peak area of the product in percentage (*P*%) is defined by Equation 1.

$$P\% = A_{prod}/(A_{subs} + A_{prod}) \times 100 \quad (1)$$

in which A_{subs} and A_{prod} represents the integrated peak area for 1-formylpyrrolidine (substrate) and 1-formyl-2-methoxypyrrolidine (product), respectively. *P*% is equivalent to GC yield, assuming that the reaction does not generate significant amount of by-products under these reaction conditions; this assumption seems to be justified since the reaction has been extensively studied and is known to progress cleanly under the conditions used and our GC analysis showed no by-products.

As shown in Figure 3, there were no significant differences in *P*% between the separate experiments with the same applied current. The relative standard deviations for *P*% are 2.9% and 0.7%, respectively, for the 6 experiments carried out at 0.16 A and 0.32 A. The peak heights of both the substrate and the product were also examined for each experiment, and no evidence was found for any effect of gas bubbles in the sample loop during the injection.

We then made measurements on the methoxylation of 1-formylpyrrolidine over a range of flow rates (0.5 to 3 cm^3 min^{-1}) and currents to validate the performance of the electrochemical reactor and the GC sampling method. Hexanenitrile (1.00 g dm^{-3}) was added to the MeOH solution as an internal standard, with 1-formylpyrrolidine (0.1 mol dm^{-3}) and $[Et_4N][BF_4]$ (0.05 mol dm^{-3}). The masses of 1-formylpyrrolidine and 1-formyl-2-methoxypyrrolidine were calculated from the linear calibration curves of the corresponding compounds. Table 1 lists the reaction conditions, fractional conversion, fractional selectivity, current efficiency and product formation rate. Our measured fractional conversion and fractional selectivity are in good agreement with the experimental results published previously by Brown and his co-workers.[49] The currents range from 0.62 to 1.5 A, and the current ratio (*R*) for each experiment is also given in Table 1. The current ratio is defined as the ratio of the current applied to the electrochemical reactor (I_a) to the current theoretically required to achieve a full conversion (I_t), see Equation 2. I_t is calculated from Faraday's laws of electrolysis.

$$R = I_a/I_t = I_a/(n\mathrm{F}Q_v\, c) \quad (2)$$

where *n* is the number of electrons required to convert a single substrate molecule at the working electrode, F is the Faraday constant, Q_v represents the volumetric flow rate of the substrate solution, and *c* is the concentration of the substrate at the entrance of the continuous-flow electrochemical reactor.

At the exit of a continuous-flow electrochemical reactor, the fractional conversion (X) is related to both I_a and I_t.[34, 52] When I_a is smaller than I_t, full conversion cannot be achieved, and fractional conversion is proportional to R, provided that there are no side reactions occurring on the surface of the working electrode and that the reaction is under diffusion control. When $I_a > I_t$, competing reactions will occur, not only decreasing the current efficiency, but potentially reducing the selectivity of the desired reaction. Moreover, the higher I_a is, the larger the applied electric potential, leading to a greater probability of decomposition of the solvent and the supporting electrolyte and over-oxidation/reduction of the product. Therefore, for electrochemical synthesis, the optimal current should be as close as possible to the I_t of a reaction system for a given Q_v and c.

From the experimental point of view, we have selected R as an independent factor to optimise in a continuous-flow electrochemical reactor since I_t is a function of both Q_v and c. However, the same approach does not apply to optimising using I_a since different R values are produced when Q_v and c are varied, see Equation 2. As a result, the same value of I_a might be close to I_t for one value of $Q_v \times c$ but far away from I_t for another value of $Q_v \times c$. For an optimisation process involving a wide range of Q_v and c, selecting R as the independent factor allows tests to be avoided if they are in a region far away from $R = 1$. By contrast, when the current is used as the independent factor, eliminating the tests under very unfavourable conditions can only be achieved by imposing multiple constraints to the numerical optimisation procedure.

According to Equation 2 and the discussion above, it is clear that Q_v, c and R (or I_a) are not completely uncorrelated when using them as the factors to optimise an electrochemical reaction. However, c can have either a strong or weak effect on the chemistry, the diffusion, and the adsorption/desorption of a range of species on the surfaces of electrodes. Together with the effects of Q_v and the geometry of the flow reactor on the residence time, neither conversion nor yield can be easily correlated to Q_v and c using the simple relationship reported in the literature.[52] In this study, we regard our continuous-flow electrochemical reactor as a black box; and hence Q_v, c and R are selected as the independent factors for testing optimisation processes.

Our third test on the methoxylation of 1-formylpyrrolidine system was a two-dimensional test where the parameters were stepped to profile the response surface. In the test the flow rate and the current ratio varied in the ranges of 1.0-3.0 $cm^3\ min^{-1}$ and 0.6-1.4, respectively with step sizes of 1 $cm^3\ min^{-1}$, and 0.1. P% (equivalent to GC yield, see Equation 1) was measured as a function of the flow rate and the current ratio, and is presented as a 3-D plot in Figure 4a, which shows that the response surface only has a single maximum in the studied range. The best experimental conditions were found at 1.0 $cm^3\ min^{-1}$ and $R = 1.4$, giving a P% of 93%.

As expected, the absolute values of *P*% are different from those of the calibrated yield shown in Table 1. These differences are attributed firstly to the different GC (FID) response factors of 1-formylpyrrolidine and 1-formyl-2-methoxypyrrolidine and also to the differences in the volatility of the two compounds in the GC sample loop. Nevertheless, we have found that for the methoxylation reaction in this study, *P*% is sufficient to be used as the response to locate the optimised experimental conditions. One of the advantages of using *P*% instead of the true yield is that it is not necessary to add any internal standard to the reaction solution. This is important because it is not trivial to find a GC internal standard which does not become involved in any electrochemical reactions, either at working and counter electrodes under the relatively high cell voltage used in these experiments. In addition to inertness, other aspects which need to be considered when choosing an internal standard, include low cost, high volatility and not co-eluting with other analytes. Therefore, there are clear advantages in removing the need for an internal standard.

Figure 4b shows the two-factor optimisation of the methoxylation of 1-formylpyrrolidine using the SNOBFIT (Stable Noisy Optimisation by Branch and FIT) algorithm[53] and *P*% as the response to optimise (see Table 1).

In every reaction optimisation, one has to define the multi-dimensional parameter space for optimisation; this definition is usually based on any knowledge of the reaction, the reactor, the sensitivity of the analytical method, and the cost of reagents. In the particular case of a continuous-flow electrochemical synthesis, mass transport as dictated by the geometry of the reactor imposes a limit to the conversion at the exit for a given reactor. Moreover, if the current ratio (defined in Equation 2) is much higher than 1, a variety of side reactions may occur, which may lead to poorly-soluble by-products blocking reactors and sampling devices.

The optimisation was repeated for 26 experiments. The highest value of *P*% (89%) was achieved at a flow rate of 1.0 cm^3 min^{-1} and current ratio of 1.36, as indicated by an arrow in Figure 4b. Clearly, the optimal conditions found by the SNOBFIT algorithm are consistent with the results located by the previous test (Figure 4a). Also it can be seen from Figure 4b that the algorithm focused on locating optimal conditions during the optimisation; hence more tests were made in the region near the optimal conditions while, at the same time, it randomly explored the empty space to maximise the probability of finding the global optimum. A global optimum is the extrema (minimum or maximum) of the objective function for the entire input search space.

The electrochemical oxidation of 3-bromobenzyl alcohol

Next we focussed on the electrochemical oxidation of 3-bromobenzyl alcohol in acetonitrile (MeCN) solution with $[Et_4N][BF_4]$ again as the supporting electrolyte, Scheme 2. Unlike the methoxylation of 1-formylpyrrolidine in MeOH, water was added to MeCN as a co-solvent/reactant, where reduction of H_2O provides a suitable counter electrode reaction, generating H_2 gas. For all of the tests on the oxidation of 3-bromobenzyl alcohol, the concentration of H_2O was kept at 50 g dm^{-3} in MeCN. The working electrode (anode) was a platinum sheet; and the counter electrode (cathode) was again stainless steel.

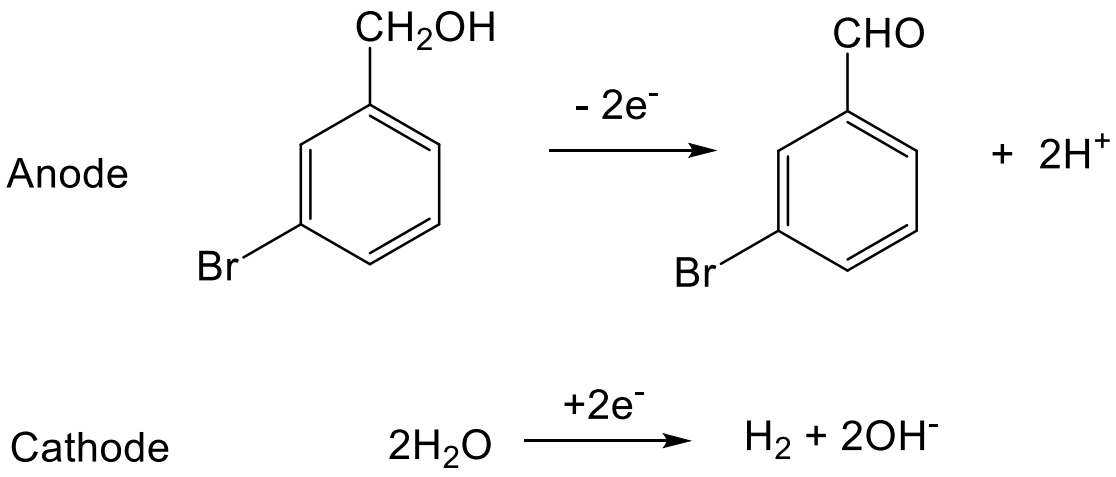

Scheme 2. Electrochemical oxidation of 3-bromobenzyl alcohol.

Our initial tests were carried out using the apparatus configured for GC analysis (Figures 1b and 2a) but we found that, in the presence of water and $[Et_4N][BF_4]$, 3-bromobenzyl alcohol could not be vaporised in the GC sample loop and/or in the GC injector. Furthermore, there was poor reproducibility of the GC measurements on 3-bromobenzylaldehyde. Possible reasons for the troublesome GC measurements are the low volatility of 3-bromobenzyl alcohol and the strong interactions between 3-bromobenzyl alcohol, water and $[Et_4N][BF_4]$ (Note that the estimated normal boiling point is about 65 °C higher for 3-bromobenzyl alcohol than for 1-formylpyrrolidine, making 3-bromobenzyl alcohol much more challenging for GC analysis.)

Therefore, we moved to the IR method. Figure 5a shows the IR spectra recorded by the ReactIR spectrometer for both 3-bromobenzyl alcohol and 3-bromobenzylaldehyde. The product has a strong absorption band at 1700

cm^{-1} which does not overlap with any bands of the substrate, making it suitable for quantifying the concentration of 3-bromobenzylaldehyde in the reaction solutions. However, it is almost impossible to use FTIR to quantify the starting material, 3-bromobenzyl alcohol, because all of its absorption bands between 750 and 2000 cm^{-1} are overlapped by those of the product 3-bromobenzylaldehyde. Moreover, given the efficiency of the reaction, particularly at the experimental conditions near the optimal conditions, the concentration of residual 3-bromobenzyl alcohol in the solution is too low to be accurately measured using ATR-IR. As a result, we only used FTIR to quantify the concentration of 3-bromobenzylaldehyde in the reaction solutions.

To develop a reliable IR method for determining the concentration of 3-bromobenzylaldehyde, we first investigated the changes to the IR background during the optimisation process. This is important because ATR-FTIR is potentially highly sensitive to surface contamination which could build up during a reaction. Therefore, our IR measurements were carried out in two stages. For the first stage, a reference solution (50 g dm^{-3} H_2O and 0.05 mol dm^{-3} $[Et_4N][BF_4]$ in MeCN) was flowed onto the IR probe and the spectra were recorded to serve as the background spectrum. Then, the solution was switched to the reaction solution from the reactor, containing a mixture of the product and by-products. After 20 minutes, the solution was switched back to the reference solution. This procedure was repeated >60 times, showing that the baseline absorbance increased by ~0.019 at 1700 cm^{-1} between the first and last spectrum. This change is comparable to the expected peak height obtained from a low concentration of 3-bromobenzylaldehyde (e.g. A = 0.011 at 1700 cm^{-1} for a solution with 0.028 mol dm^{-3} of 3-bromobenzylaldehyde, see Figure 5b). Therefore, we concluded that, for reliable results, an IR background spectrum should be recorded between each sample spectrum and this procedure was used when a reaction was being optimised using the IR configuration, even though collecting both the background and the sample spectra doubles the experimental time required for each test.

After the corresponding background spectrum had been subtracted, a two-point base line correction was applied to the data. Figure 5d shows a typical IR spectrum of the reaction solution between 1636 cm^{-1} and 1928 cm^{-1}. Apart from the strong carbonyl peak at ~1700 cm^{-1}, two shoulders can be clearly identified at 1716 cm^{-1} and 1741 cm^{-1}, assigned to by-products of the oxidation of 3-bromobenzyl alcohol. A peak fitting algorithm[54] was applied to fit the peaks in the region of 1636-1928 cm^{-1}. For simplicity in the first approximation, all peaks were assumed to be Lorentzian; and no constraints were applied to either peak position or peak width. The initial number of the peaks in the above region was set to 3. If one of the fitted peaks had very small peak height (<0.001) or very large peak width (>100 cm^{-1}), the total number of the peaks was decreased by 1, and the entire peak fitting process was then restarted. All of this analysis was carried out automatically by the software during the

optimisation. The height of the peak at ~1700 cm^{-1} was then used to calculate the concentration of the 3-bromobenzylaldehyde using the calibration curve presented in Figure 5c. Together with the known concentration of the substrate, the percentage yield of the oxidation reaction was calculated for each test.

We selected three factors (the concentration of 3-bromobenzyl alcohol, the total flow rate, and the current ratio) to optimise the oxidation of 3-bromobenzyl alcohol using the SNOBFIT algorithm. The low and upper limits for each factor are listed in Table 3. We used the yield of 3-bromobenzylaldehyde as the response to optimise and the yield was measured after the system had reached a steady-state for each test, usual after 10-20 minutes.

Figure 6 shows the results of the yield optimisation of the oxidation of 3-bromobenzyl alcohol (Scheme 2). The colour map represents the percentage yield. A total of 4 tests were made for each iteration. The 4 testing conditions in the first iteration were selected completely randomly. The subsequent test conditions were generated iteratively by the SNOBFIT algorithm based on the percentage yield (response) obtained from the previous tests. The reaction conditions and the percentage yield of the full data set are listed in Table S1 in supplemental material.

The optimum conditions were found to be 0.03 mol dm^3 for the concentration of 3-bromobenzyl alcohol, 0.9 cm^3 min^{-1} for the flow rate, and 1.3 for the current ratio, giving the highest percentage yield of 68%. The SNOBFIT algorithm made more tests in the low concentration and high current ratio region because this was the region where a local optimum had been found. The algorithm had also explored other parts of the 3-D parameter space with high concentration and low current ratio (see the blue/light blue spheres in Figure 6) in an unsuccessful attempt to find possible global optimum in this region.

It has been discussed in the literature[51] that, assuming 100% charge efficiency, conversion is inversely proportional to the flow rate for given current and concentration. In our experiments, the current ratio rather than the current was used as the independent parameter. This means that the relationship between the conversion and the flow rate is different. In order to maintain the same current ratio, a higher current would be applied when increasing the flow rate according to Equation 2, and hence the inverse effect of the high flow rate on the conversion would be partially compensated by keeping the current ratio constant. Furthermore, the percentage yield is also related to the selectivity, which is a complex function of residence time, flow rate and applied current/voltage. Therefore, we did not observe any simple correlation between flow rate and percentage yield at a fixed concentration.

The reliability of the optimisation process is mainly dependent on the robustness, reproducibility and accuracy of the analytical technique employed. In the case of the oxidation of 3-bromobenzyl alcohol, we have found that our peak fitting approach appears to be the most robust method for processing the IR data. The ν(C-O) bands from the unknown by-products vary in their wavenumber and are also affected by noise in the IR spectrum as well as by the concentration of the by-products. Our peak fitting method, however, focuses on information from the strongest ν(C-O) peaks at ~1700 cm^{-1}, largely removing the interference from those by-products. From our experiments, the fitted peaks for 3-bromobenzylaldehyde have an average peak centre at 1699.3 ±0.7 cm^{-1} and an average peak width of 24.3 ±1.7 cm^{-1} across the 69 different spectra collected during optimisation. These values compare well with the peak centre (1700 cm^{-1}) and the peak width (25.7±0.4) obtained from 5 solutions with pure 3-bromobenzylaldehyde (Figure 5b). Thus we conclude that the fitted peak at ~1700 cm^{-1} has the same characteristics as the carbonyl peak of pure 3-bromobenzylaldehyde.

Conclusions

In this paper, we have presented a new self-optimising apparatus used for continuous-flow electrochemical synthesis. The performance and the reliability of this self-optimising system have been demonstrated with two selected reactions: the electrochemical methoxylation of 1-formylpyrrolidine and the electrochemical oxidation 3-bromobenzyl alcohol.

A reliable and efficient in-line gas-liquid separator is crucial to integrate real-time, online analytical technologies with a flow electrochemical reactor. We have described two, new computer-controlled gas-liquid separators: one for GC and the other for ATR-FTIR, which have been constructed in-house from relatively simple components. In particular, we have shown that the integrated gas-liquid separator for ATR-FTIR enables both gas separation and ATR-FTIR spectroscopy sampling to be carried out simultaneously in a single simple device. Because of the high surface tension of the liquid, the ATR-FTIR probe only records the spectrum from the liquid phase, even though the immersion IR probe is surrounded by gas.

Within the context of continuous-flow electrochemistry, ATR-FTIR has several advantages over GC: (i) ATR-FTIR is suitable for non-volatile substrates and products; (ii) there is no need for internal standards, which may be difficult to find for electrochemical synthesis systems; and (iii) ATR-FTIR makes it easy to identify the steady state for a continuous-flow reactor. The design of the integrated gas-liquid separator for ATR-FTIR could also be applied to the other analytical techniques for reaction monitoring in continuous-flow electrochemical reactors, for instance, Raman spectroscopy, where optical fibre probes are readily available. Since the gas-liquid

two-phase flow in reactors is quite common on both laboratory and industrial scales, our two designs of gas-liquid separator could provide simple approaches for incorporating process analytical technology into other two-phase flow reactors.

Additionally, we have shown that apart from the common factors (e.g. the flow rate and the concentration of the substrate), the current ratio may be a preferable factor for the self-optimisation of electrochemical reactors rather than the current itself because the ratio can reduce the number of the tests required. The continuous-flow reactor is treated as a 'black box' and the correlations between a range of factors are not clear for the optimisation of a given electrochemical reaction. SNOBFIT has been shown to be a useful algorithm for optimising electrochemical reactions in a continuous-flow reactor because the random search part of the algorithm increases the chances of finding the global maximum of the response (e.g. the percentage yield of the product).

Of course, ATR-FTIR also has limitations in sensitivity and peak overlapping. However, sensitivity is less likely to be a problem for a multigram electrochemical reactor such as the Ammonite because the concentration of products is high enough for easy detection by ATR-FTIR. As regards peak overlapping, we have shown that a simple peak fitting algorithm can be an effective and robust method for overcoming this problem at least for the oxidation reaction of 3-bromobenzyl alcohol. Since this may not be the case for the other reactions, we are currently developing this approach further for use in conjunction with our self-optimising reactors.

Acknowledgements

We are grateful financial support from the EPSRC Programme Grant (EP/P013341/1) and from Hermes Fellowships Call 17 (JK) at the University of Nottingham and Eli Lilly and Company through the Lilly Research Awards Program (KEJ). We thank Mr. J. Warren and Mr. C. Howell-Bennett for designing and making the gas-liquid separators. We also thank Messrs. M. Guyler, R. Wilson, R. Meehan, D. Litchfield, C. Dixon, and M. Dellar for their technical assistance, and to Mr. Adrian Burke from Mettler-Toledo for his support and helpful advice.

References

1. A. Rojko. "Industry 4.0 Concept: Background and Overview". International Journal of Interactive Mobile Technologies (iJIM). 2017. 11(5): 77.
2. K. Plumb. "Continuous Processing in the Pharmaceutical Industry: Changing the Mind Set". Chem. Eng. Res. Des. 2005. 83(6): 730-738.
3. S. L. Lee, T. F. O'Connor, X. Yang, C. N. Cruz, S. Chatterjee, R. D. Madurawe, C. M. V. Moore, L. X. Yu, and J. Woodcock. "Modernizing Pharmaceutical Manufacturing: from Batch to Continuous Production". J. Pharm. Innov. 2015. 10(3): 191-199.
4. S. Bordawekar, A. Chanda, A. M. Daly, A. W. Garrett, J. P. Higgins, M. A. LaPack, T. D. Maloney, J. Morgado, S. Mukherjee, J. D. Orr, G. L. Reid, B.-S. Yang, and H. W. Ward. "Industry Perspectives on Process Analytical Technology: Tools and Applications in API Manufacturing". Org. Process Res. Dev. 2015. 19(9): 1174-1185.
5. L. X. Yu, G. Amidon, M. A. Khan, S. W. Hoag, J. Polli, G. K. Raju, and J. Woodcock. "Understanding Pharmaceutical Quality by Design". AAPS J. 2014. 16(4): 771-783.
6. P. Sagmeister, J. D. Williams, C. A. Hone, and C. O. Kappe. "Laboratory of the future: a modular flow platform with multiple integrated PAT tools for multistep reactions". React. Chem. Eng. 2019. 4(9): 1571-1578.
7. S. Krishnadasan, R. J. C. Brown, A. J. deMello, and J. C. deMello. "Intelligent routes to the controlled synthesis of nanoparticles". Lab Chip. 2007. 7(11): 1434-1441.
8. J. P. McMullen, M. T. Stone, S. L. Buchwald, and K. F. Jensen. "An Integrated Microreactor System for Self-Optimization of a Heck Reaction: From Micro- to Mesoscale Flow Systems". Angew. Chem. Int. Ed. 2010. 49(39): 7076-7080.
9. J. P. McMullen and K. F. Jensen. "An Automated Microfluidic System for Online Optimization in Chemical Synthesis". Org. Process Res. Dev. 2010. 14(5): 1169-1176.
10. R. A. Bourne, R. A. Skilton, A. J. Parrott, D. J. Irvine, and M. Poliakoff. "Adaptive Process Optimization for Continuous Methylation of Alcohols in Supercritical Carbon Dioxide". Org. Process Res. Dev. 2011. 15(4): 932-938.
11. C. Houben and A. A. Lapkin. "Automatic discovery and optimization of chemical processes". Curr. Opin. Chem. Eng. 2015. 9: 1-7.

12. D. C. Fabry, E. Sugiono, and M. Rueping. "Online monitoring and analysis for autonomous continuous flow self-optimizing reactor systems". React. Chem. Eng. 2016. 1(2): 129-133.

13. A. Gioiello, V. Mancino, P. Filipponi, S. Mostarda, and B. Cerra. "Concepts and Optimization Strategies of Experimental Design in Continuous-Flow Processing". J. Flow Chem. 2016. 6(3): 167-180.

14. B. J. Reizman and K. F. Jensen. "Feedback in Flow for Accelerated Reaction Development". Acc. Chem. Res. 2016. 49(9): 1786-1796.

15. V. Sans and L. Cronin. "Towards dial-a-molecule by integrating continuous flow, analytics and self-optimisation". Chem. Soc. Rev. 2016. 45(8): 2032-2043.

16. M. B. Plutschack, B. Pieber, K. Gilmore, and P. H. Seeberger. "The Hitchhiker's Guide to Flow Chemistry(II)". Chem. Rev. 2017. 117(18): 11796-11893.

17. P. S. Gromski, A. B. Henson, J. M. Granda, and L. Cronin. "How to explore chemical space using algorithms and automation". Nat. Rev. Chem. 2019. 3(2): 119-128.

18. R. A. Bourne, K. K. Hii, and B. J. Reizman. "Introduction to Synthesis 4.0: towards an internet of chemistry". React. Chem. Eng. 2019. 4(9): 1504-1505.

19. B. M. Wyvratt, J. P. McMullen, and S. T. Grosser. "Multidimensional dynamic experiments for data-rich process development of reactions in flow". React. Chem. Eng. 2019. 4(9): 1637-1645.

20. C. Waldron, A. Pankajakshan, M. Quaglio, E. Cao, F. Galvanin, and A. Gavriilidis. "An autonomous microreactor platform for the rapid identification of kinetic models". React. Chem. Eng. 2019. 4(9): 1623-1636.

21. C. Schenk, M. Short, J.S. Rodriguez, D. Thierry, L.T. Biegler, S. García-Muñoz, W. Chen. "Introducing KIPET: A novel open-source software package for kinetic parameter estimation from experimental datasets including spectra". Comput. Chem. Eng. 2020. 134: 106716.

22. A. D. Clayton, J. A. Manson, C. J. Taylor, T. W. Chamberlain, B. A. Taylor, G. Clemens, and R. A. Bourne. "Algorithms for the self-optimisation of chemical reactions". React. Chem. Eng. 2019. 4(9): 1545-1554.

23. V. Rosso, J. Albrecht, F. Roberts, and J. M. Janey. "Uniting laboratory automation, DoE data, and modeling techniques to accelerate chemical process development". React. Chem. Eng. 2019. 4(9): 1646-1657.

24. D. Cambie, C. Bottecchia, N. J. W. Straathof, V. Hessel, and T. Noel. "Applications of Continuous-Flow Photochemistry in Organic Synthesis, Material Science, and Water Treatment". Chem. Rev. 2016. 116(17): 10276-10341.

25. M. Chen, M. Zhong, and J. A. Johnson. "Light-Controlled Radical Polymerization: Mechanisms, Methods, and Applications". Chem. Rev. 2016. 116(17): 10167-10211.

26. A. A. Ghogare and A. Greer. "Using Singlet Oxygen to Synthesize Natural Products and Drugs". Chem. Rev. 2016. 116(17): 9994-10034.

27. M. D. Karkas, J. A. Porco, and C. R. J. Stephenson. "Photochemical Approaches to Complex Chemotypes: Applications in Natural Product Synthesis". Chem. Rev. 2016. 116(17): 9683-9747.

28. D. Ravelli, S. Protti, and M. Fagnoni. "Carbon-Carbon Bond Forming Reactions via Photogenerated Intermediates". Chem. Rev. 2016. 116(17): 9850-9913.

29. R. Remy and C. G. Bochet. "Arene-Alkene Cycloaddition". Chem. Rev. 2016. 116(17): 9816-9849.

30. N. A. Romero and D. A. Nicewicz. "Organic Photoredox Catalysis". Chem. Rev. 2016. 116(17): 10075-10166.

31. K. L. Skubi, T. R. Blum, and T. P. Yoon. "Dual Catalysis Strategies in Photochemical Synthesis". Chem. Rev. 2016. 116(17): 10035-10074.

32. M. Atobe, H. Tateno, and Y. Matsumura. "Applications of Flow Microreactors in Electrosynthetic Processes". Chem. Rev. 2018. 118(9): 4541-4572.

33. K. Mitsudo, Y. Kurimoto, K. Yoshioka, and S. Suga. "Miniaturization and Combinatorial Approach in Organic Electrochemistry". Chem. Rev. 2018. 118(12): 5985-5999.

34. D. Pletcher, R. A. Green, and R. C. D. Brown. "Flow Electrolysis Cells for the Synthetic Organic Chemistry Laboratory". Chem. Rev. 2018. 118(9): 4573-4591.

35. T. Noel, Y. Cao, and G. Laudadio. "The Fundamentals Behind the Use of Flow Reactors in Electrochemistry". Acc. Chem. Res. 2019. 52(10): 2858-2869.

36. K. Poscharny, D. C. Fabry, S. Heddrich, E. Sugiono, M. A. Liauw, and M. Rueping. "Machine assisted reaction optimization: A self-optimizing reactor system for continuous-flow photochemical reactions". Tetrahedron. 2018. 74(25): 3171-3175.

37. J. A. Manson, A. D. Clayton, C. G. Niño, R. Labes, T. W. Chamberlain, A. J. Blacker, N. Kapur, and R. A. Bourne. "A Hybridised Optimisation of an Automated Photochemical Continuous Flow Reactor". CHIMIA. 2019. 73(10): 817-822.

38. Z. Qiu, C. W. Tai, G. A. Niklasson, and T. Edvinsson. "Direct observation of active catalyst surface phases and the effect of dynamic self-optimization in NiFe-layered double hydroxides for alkaline water splitting". Energy Environ. Sci. 2019. 12(2): 572-581.

39. D. N. Jumbam, R. A. Skilton, A. J. Parrott, R. A. Bourne, and M. Poliakoff. "The effect of self-optimisation targets on the methylation of alcohols using dimethyl carbonate in supercritical CO_2". J. Flow Chem. 2012. 2: 24-27.

40. R. A. Skilton, A. J. Parrott, M. W. George, M. Poliakoff, and R. A. Bourne. "Real-time feedback control using online attenuated total reflection fourier transform infrared (ATR FT-IR) spectroscopy for continuous flow optimization and process knowledge". Appl. Spectrosc. 2013. 67(10): 1127-1131.

41. Z. Amara, E. S. Streng, R. A. Skilton, J. Jin, M. W. George, and M. Poliakoff. "Automated Serendipity with Self-Optimizing Continuous-Flow Reactors". Eur. J. Org. Chem. 2015. 2015(28): 6141-6145.

42. R. A. Skilton, R. A. Bourne, Z. Amara, R. Horvath, J. Jin, M. J. Scully, E. Streng, S. L. Y. Tang, P. A. Summers, J. Wang, E. Perez, N. Asfaw, G. L. P. Aydos, J. Dupont, G. Comak, M. W. George, and M. Poliakoff. "Remote-controlled experiments with cloud chemistry". Nat. Chem. 2015. 7(1): 1-5.

43. A. J. Parrott, R. A. Bourne, G. R. Akien, D. J. Irvine, and M. Poliakoff. "Self-Optimizing Continuous Reactions in Supercritical Carbon Dioxide". Angew. Chem., Int. Ed. 2011. 50(16): 3788-3792.

44. E. S. Streng, D. S. Lee, M. W. George, and M. Poliakoff. "Continuous N-alkylation reactions of amino alcohols using gamma-Al2O3 and supercritical CO2: unexpected formation of cyclic ureas and urethanes by reaction with CO2". Beilstein J Org Chem. 2017. 13: 329-337.

45. N. Holmes, G. R. Akien, A. J. Blacker, R. L. Woodward, R. E. Meadows, and R. A. Bourne. "Self-optimization of the final stage in the synthesis of EGFR kinase inhibitor AZD9291 using an automated flow reactor". React. Chem. Eng. 2016. 1(4): 366-371.

46. N. Holmes, G. R. Akien, R. J. D. Savage, C. Stanetty, I. R. Baxendale, A. J. Blacker, B. A. Taylor, R. L. Woodward, R. E. Meadows, and R. A. Bourne. "Online quantitative mass spectrometry for the rapid adaptive optimisation of automated flow reactors". React. Chem. Eng. 2016. 1(1): 96-100.

47. M. I. Jeraal, N. Holmes, G. R. Akien, and R. A. Bourne. "Enhanced process development using automated continuous reactors by self-optimisation algorithms and statistical empirical modelling". Tetrahedron. 2018. 74(25): 3158-3164.

48. R. A. Green, R. C. D. Brown, and D. Pletcher. "Electrosynthesis in extended channel length microfluidic electrolysis cells". J. Flow Chem. 2016. 6(3): 191-197.

49. R. A. Green, R. C. D. Brown, D. Pletcher, and B. Harji. "An extended channel length microflow electrolysis cell for convenient laboratory synthesis". Electrochem. Commun. 2016. 73: 63-66.

50. R. A. Green, K. E. Jolley, A. A. M. Al-Hadedi, D. Pletcher, D. C. Harrowven, O. De Frutos, C. Mateos, D. J. Klauber, J. A. Rincon, and R. C. D. Brown. "Electrochemical Deprotection of para-Methoxybenzyl Ethers in a Flow Electrolysis Cell". Org. Lett. 2017. 19(8): 2050-2053.

51. R. A. Green, R. C. D. Brown, D. Pletcher, and B. Harji. "A Microflow Electrolysis Cell for Laboratory Synthesis on the Multigram Scale". Org. Process Res. Dev. 2015. 19(10): 1424-1427.

52. R. A. Green, R. C. D. Brown, and D. Pletcher. "Understanding the performance of a microfluidic electrolysis cell for routine organic electrosynthesis". J. Flow Chem. 2015. 5(1): 31-36.

53. W. Huyer and A. Neumaier. "SNOBFIT -- Stable Noisy Optimization by Branch and Fit". Association for Computing Machinery, 2008.

54. T. C. O'Haver. "Pragmatic Introduction to Signal Processing: Applications in scientific measurement". 2018.

Figure captions

Figure 1. A schematic diagram of the electrochemical synthesis flow apparatus for use with GC and ATR-FTIR in-line analysis. (a) Reactor and the delivery unit of reaction solutions. Parts are labelled as follows: DPS, dc power supplier; ER, Ammonite electrochemical reactor; M, mixer; P, pressure transducer; PI, pressure indicator; PC, personal computer; PU1, PU2, HPLC pump; S1, S2, solution reservoir; V, shut-off valve; TP, Swagelok T-piece. (b) Downstream unit for use with GC: CG, carrier gas inlet; CO, carrier gas inlet to GC; GC, gas chromatography; GLS, gas-liquid separator, see Figure 2a for details; H_2, hydrogen gas vent; IV, sample injection valve. (c) Downstream unit for use with ATR-FTIR: GLS, gas-liquid separator, see Figure 2b for details; H_2, hydrogen gas to the exhaust pipe; IR, ReactIR spectrometer; PP, peristaltic pump; PU3, HPLC pump; R-IP, ReactIR ATR immersion probe; S3, reference solution reservoir; SV, computer-controlled switching valve; V3,V4, shut-off valves. The solid lines (in black) represent the pipes containing the fluids (e.g. solvents, reactants, products). The dashed lines in blue represent electrical cables between the devices and between the device and the computer.

Figure 2. Gas-liquid separators (GLS) for use with GC and ATR-FTIR analysis (see main text for a description of their operation). (a) Schematic diagram of the GLS for GC, G, gas: GC, gas chromatography; GT; transparent glass tube; HE, heat exchanger; L, liquid; LLD, liquid-level detector; PC, personal computer; PP, peristaltic pump; PR, product reservoir; PU3, HPLC pump. (b) Schematic diagram of the GLS for ATR-FTIR G, gas; I, inlet pipe; L, liquid; OG, outlet pipe for gas; OL, outlet pipe for liquid; R-IP, ReactIR probe. (c) Photo of the GLS shown in (b). The ReactIR probe is placed at an angle to the inlet pipe, to accelerate the flow over the ATR-FTIR sensing surface, and hence to reduce the waiting time required for obtaining reproducible spectra after switching to a fluid with a different composition.

Figure 3. Traces showing the reproducibility of the GC analysis on the samples after H_2 gas had been separated from the product streams by using the gas-liquid separator shown in Figure 2a. *P*% represents the integrated peak area of the product in percentage, calculated from the GC chromatograms using Equation 1. 0.16 A and 0.32 A are the currents applied to the electrochemical reactor during the reactions. The flow rate was kept at 1 cm^3 min^{-1}. The concentrations for 1-formylpyrrolidine and $[Et_4N][BF_4]$ are 0.1 mol dm^{-3} and 0.05 mol dm^{-3}, respectively.

Figure 4. (a) The response surface of the methoxylation of 1-formylpyrrolidine measured by GC. (b) Two-factor optimisation of the methoxylation of 1-formylpyrrolidine using the SNOBFIT algorithm: factor 1, flow rate; factor 2, current ratio. The optimised condition is indicated by the black arrow at the top centre of the figure. The x-, y-, z-axes represent flow rate, current ratio and integrated peak area of the product in percentage (*P*%), calculated from the GC chromatograms using Equation 1. The concentrations of 1-formylpyrrolidine and [Et4N][BF4] are 0.1 mol dm^3 and 0.05 mol dm^3, respectively. (See also Table 1).

Figure 5. (a) IR spectra of 3-bromobenzyl alcohol (A) and 3-bromobenzylaldehyde (B) after subtraction of the corresponding reference spectra. The concentration of 3-bromobenzyl alcohol and 3-bromobenzylaldehyde are 0.25 mol dm^{-3} and 0.29 mol dm^{-3}, respectively. (b) IR spectra of 3-bromobenzylaldehyde at five concentrations. (c) the calibration curve for 3-bromobenzylaldehyde, plotted as the concentration of 3-bromobenzylaldehyde against the peak height at 1700 cm^{-1}. (d) Peak fitting in the range between 1636 and 1928 cm^{-1} after the base line correction. The solid black line and the dashed red line represent the experimental and the fitted spectrum, respectively. All peaks are assumed to be Lorentzian. The peak at ~1700 cm^{-1} is assigned as the ν(C-O) absorption

band of the product, 3-bromobenzylaldehyde. The two arrows indicate the two *ν*(C-O) absorption bands, possibly resulting from as yet unidentified by-products.

Figure 6. Three-factor optimisation of the oxidation reaction of 3-bromobenzyl alcohol using the SNOBFIT algorithm. The x-, y-, z-axes are the flow rate, the concentration of 3-bromobenzyl alcohol substrate, and the current ratio, respectively. The units for the flow rate and the concentration are cm^3 min^{-1} and mol dm^{-3}, respectively. The colour of the spots indicates the percentage yield of 3-bromobenzylaldehyde product (red high, blue low) and the length of the stem is merely related to the value of the current ratio. The optimised conditions are indicated by the black arrow. The concentration of $[Et_4N][BF_4]$ was 0.05 mol dm^{-3}.

Table 1. Performance of ammonite electrolysis flow reactor for the methoxylation of 1-formylpyrrolidine [a,b]

Entry No.	No. repeated experiments	Flow rate	Applied current	Current ratio	Fractional conversion [c, d]	Fractional selectivity [c, d]	Current efficiency,%	Product formation rate
		(cm^3 min^{-1})	(A)	-	-	-	-	g $hour^{-1}$
1	6	0.5	0.10	0.62	0.50±0.04	0.90±0.09	72±6%	0.17
2	6	0.5	0.16	1.00	0.80±0.02	0.97±0.04	70±4%	0.30
3	6	0.5	0.20	1.24	0.88±0.01	0.92±0.02	74±10%	0.31
4	4	1.0	0.40	1.24	0.84±0.01	0.95±0.05	64±2%	0.62
5	3	2.0	0.80	1.24	0.78±0.01	0.89±0.01	56±0.2%	1.1
6	2	3.0	1.5	1.55	0.85±0.004	0.81±0.01	45±1%	1.6

[a] The inlet mixtures consist of 0.05 mol dm^{-3} [Et4N][BF4] as the supporting electrolyte, 1 g dm^{-3} 1-hexanenitrile as the internal standard for GC measurements, 1-formylpyrrolidine as the reactant and MeOH as the solvent. [b] The concentration of 1-formylpyrrolidine is fixed at 0.1 mol dm^{-3}. [c] The fractional conversion and the fractional selectivity are calculated from the concentration of the starting material in the feed and the measured concentration of the starting material and the product at the outlet stream. [d] measured by GC.

Table 2. The low and upper limits for the optimisation of the methoxylation of 1-formylpyrrolidine

Factor	Name	Unit	Lower limit	Upper limit
1	Flow rate	$cm^3\ min^{-1}$	1.0	3.0
2	Current ratio	-	0.6	1.4

Table 3. The low and upper limits for the optimisation of the oxidation of 3-bromobenzyl alcohol

Factor	Name	Unit	Lower limit	Upper limit
1	Concentration of 3-bromobenzyl alcohol	$mol\ dm^{-3}$	0.03	0.23
2	Flow rate	$cm^3\ min^{-1}$	0.7	2.0
3	Current ratio	-	0.8	1.3